ORIGINAL RESEARCH ARTICLE

A Disposable Electrochemical Sensor for Lead Ion Detection Based on *In Situ* Polymerization of Conductive Polypyrrole Coating

Hengchao Zhang[1] · Yarou Li[1] · Yupan Zhang[1] · Junfeng Wu[1,2] · Shixin Li[1] · Lanlan Li[1,2]

Abstract

Lead, a toxic heavy metal, is considered one of the most serious pollutants in the water environment, posing a grave threat to human health and the global ecosystem. In this work, a simple, fast and sensitive sensor strategy for detecting trace lead ions (Pb^{2+}) in water was proposed. The disposable electrochemical sensor was fabricated with a screen-printed carbon electrode (SPCE), and the working electrode was modified in a single step with *in situ* polymerized phytic acid functionalized polypyrrole (PA-PPy). Differential pulse anodic stripping voltammetry (DPASV) was employed to realize the efficient detection of Pb^{2+} in the range of 10–600 nM with a low detection limit of 0.43 nM ($S/N = 3$). The PA-PPy@SPCE sensor exhibits good stability, repeatability and anti-interference performance, indicating a promising application for real sample detection, and satisfactory recoveries were obtained when detecting Pb^{2+} in real tap water samples. Furthermore, the rapid sensor strategy with *in situ* polymerization of phytic acid functionalized polypyrrole composite material enables large-scale Pb^{2+} sensor preparation.

Graphical Abstract
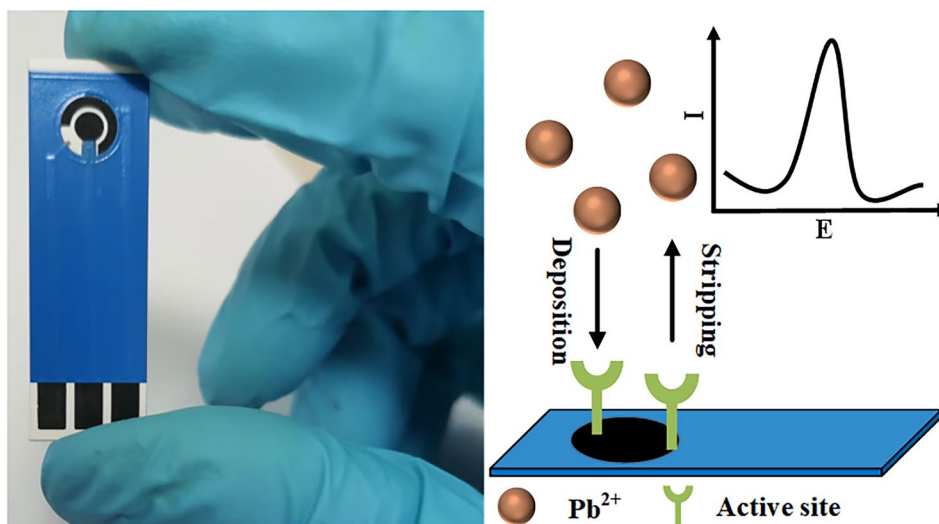
✉ Shixin Li
lishx2008@163.com

✉ Lanlan Li
lanlan.li@henau.edu.cn

Extended author information available on the last page of the article

Introduction

Heavy metals are naturally present elements that have been widely used in industry and agriculture for decades. They are metals with atomic weights ranging from 63.5 to 200.6

and densities greater than 4.5 g/cm^3.[1] Because heavy metal ions (HMIs) are very hazardous and non-biodegradable, they can accumulate in the natural environment, including in water, soil, and plants. HMIs may then enter and accumulate in the human body along with the food chain, and the toxicity of HMIs will gradually become more noticeable as their concentration rises. Therefore, even trace concentrations of HMIs can have significant negative impact on the ecosystem and its inhabitants.[2–5] It becomes even worse because the clearance rate of the human body for these HMIs is extremely low. For instance, long-term direct or indirect exposure to lead ions (Pb^{2+}) will have a variety of repercussions on the human nervous system and hematopoietic system, resulting in cardiovascular diseases, encephalopathy, anemia, and other symptoms.[6,7] The World Health Organization (WHO) has published a series of relevant documents to improving public awareness of minimum HMI intake and threshold concentrations in aquatic environments.[8] Identification and detection of HMIs in water is the basic requirement of public security at present.[9] A novel, rapid, and sensitive heavy metal detection device is urgently required to protect the environment, maintain human health, and ensure the sustainable development of society.

At present, many methods are used for the detection of HMIs, including atomic absorption spectrometry (AAS),[5] atomic fluorescence spectrometry (AFS),[10] inductively coupled plasma mass spectrometry (ICP-MS),[11] ultraviolet and visible spectrophotometry (UV),[12] x-ray,[13] and nuclear methods.[14] But they generally require expensive instruments, complex sample preparation, or professional technicians to operate.[15] In contrast, the electrochemical method has become one of the most important methods for HMI detection because of its unique advantages of simple operation, low cost, less sample consumption, high sensitivity, good selectivity, high stability, portability, low detection limit, and simultaneous detection.[16–18] Among these electrochemical methods, differential pulse anodic stripping voltammetry (DPASV) is an effective method for the detection of HMIs. It can preconcentrate the accumulated HMIs and then carry out the operation of electrochemical dissolution.[19] The interface materials on the working electrode are critical for the accumulation and electron transfer of HMIs during the electrochemical reaction[20,21] because some groups of interface materials can chelate with HMIs to promote redox reactions and improve the electron transfer rate between electrode and solution. Therefore, the selection of interface materials is an important research focus to improve the electrochemical detection performance of HMIs.[22]

Conductive polypyrrole (PPy) is a heterocyclic conjugated electronic polymer with the advantages of easy synthesis, good stability, and low cost, making it an excellent candidate for sensor interface material.[23–25] Phytic acid (PA) is a polyvalent organic acid with six phosphate groups attached to the carbon of cyclohexane, which can make phytic acid have a strong metal complex ability.[26,27] Phytic acid and its salts can effectively remove Pb and other pollutants and can be utilized as heavy metal poisoning preventive agents. Moreover, phytic acid is a green substance mainly extracted from plant tissues, which has the advantages of good biocompatibility, low toxicity, strong chelating ability and low price.[28] Therefore, combine polypyrrole and phytic acid may have the ability to enhance the perception of heavy metals.

In this work, we developed a kind of disposable electrochemical sensor with the screen printed carbon electrode (SPCE) for the rapid detection of lead ions (Pb^{2+}). *In situ* polymerized phytic acid functionalized polypyrrole (PA-PPy) was used to modify the working electrode. The PA-PPy composite was prepared rapidly and easily using the full solution method with ammonium persulfate as a strong oxidant, and phytic acid as a dopant. PA and PPy on the electrode surface can be used as electroactive materials to increase the sensor's electrochemical response signal. The results demonstrated that the PA-PPy composite materials modified electrode has a considerable electrochemical response to Pb^{2+} detection in water.

Experimental

Materials

Phytic acid (PA), ammonium persulfate (ACS reagent grade, $\geq 98.0\%$), pyrrole (reagent grade, 98.0%), isopropyl alcohol (ACS reagent grade, $\geq 99.5\%$), sodium acetate (ACS reagent grade, $\geq 99.0\%$), glacial acetic acid (ACS reagent grade, $\geq 99.7\%$) and other reagents were purchased from Sigma-Aldrich. Potassium ferrocyanide ($\geq 99.5\%$) was purchased from Tianjin Zhiyuan Chemical Reagent Co., Ltd. A lead standard solution (1000 µg/mL) was purchased from the National Non-ferrous Metals and Electronic Materials Analysis and Testing Center. Pyrrole was stored in a sealed environment at 2–8°C to prevent oxidation. As a supporting electrolyte, the HAc-NaAc buffer solution (0.1 M) was prepared by mixing a given amount of sodium acetate and acetic acid in a specific proportion. Deionized water (18.2 MΩ cm @25°C) was used throughout the experiment, and all reagents were of analytical grade. The standard solution of Pb^{2+} was diluted into different concentrations with HAc-NaAc buffer.

Apparatus

A CHI760e electrochemical workstation (CH Instrument Co., LTD, China) was used for electrochemical measurement. The Taiwan Chan Pu Company provided the SPCEs ($\Phi = 3$ mm), which consisted of three electrodes, with

carbon paste as the working electrode and the counter electrode and Ag as the reference electrode. SEM, FTIR, and ICP-MS were tested by Shiyanjia Lab (www.shiyanjia.com) with a Hitachi Regulus8100 FE-SEM instrument, Thermo Scientific Nicolet iS20, and Agilent 7850 ICP-MS instrument, respectively.

Construction of PA-PPy-Modified SPCE Sensor

PA-PPy composite materials were prepared by the full solution method. Ammonium persulfate (1.2 mmol) was dissolved in deionized water by ultrasound and labeled as A. Pyrrole monomer (1.2 mmol), isopropyl alcohol and phytic acid (0.36 mmol) were mixed evenly and marked as B. Before mixing A and B, they were refrigerated and frozen for 10 min, respectively. Then mixed solutions (2.6 μl) were dropped on the SPCE's working electrode surface to construct a PA-PPy sensor. After cooling for 10 min to ensure complete reaction, the sensor was purified with deionized water and dried at room temperature. The mixed solutions with different proportions of $V_A : V_B = 1{:}0.5$, 1:1 and 1:2 were marked as PA-PPy2, PA-PPy and PA-PPy3, respectively. The materials prepared without PA were marked as PPy.

Electrochemical Testing

Electrochemical tests were carried out on a CHI760e workstation using a three-electrode system with 0.1 M HAc-NaAc buffer electrolyte solution. The primary test method is DPASV with three processes. Firstly, the potential was set at -1.5 V while stirring to enrich Pb^{2+} on the electrode surface. Then the system was kept stationary for 30 s. Finally, a potential ranging from -1.2 V to -0.5 V was applied to dissolve Pb from the electrode into the solution without stirring. For comparison, square wave anodic stripping voltammetry (SWASV), linear sweep anodic stripping voltammetry (LSASV) and staircase anodic stripping voltammetry (SCASV) were also used to test under the same conditions.

Results and Discussion

Characterization of the PA-PPy

Figure 1 shows the SEM images of PPy and PA-PPy materials. The surface morphology of PPy is a random granular structure, and these sub-micron particles accumulate to form aggregates of several microns (Fig. 1a and b). The accumulation of these particles induces PPy to form a porous
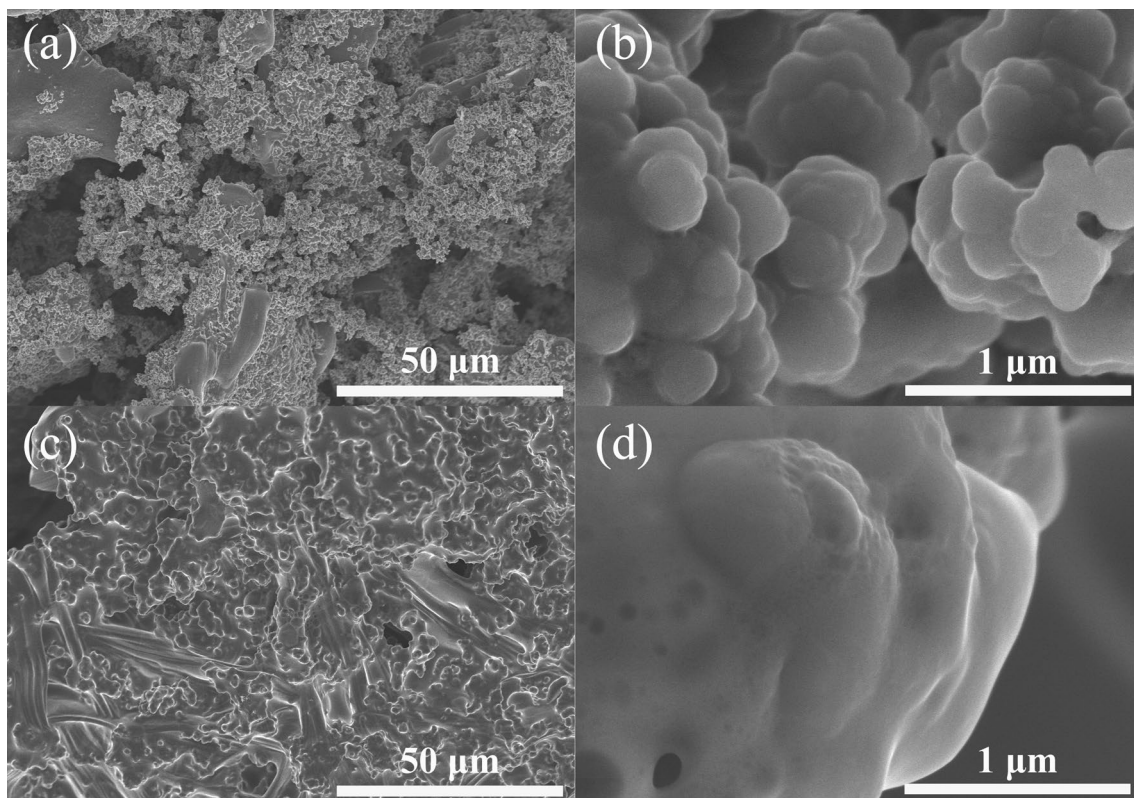

Fig. 1 SEM images of (a), (b) PPy and (c), (d) PA-PPy composites.

structure dominated by large pores, which is disadvantageous to the electron transfer. The doping of phytic acid significantly reduces the accumulation phenomena of PPy particles. These particles overlap each other to form a typical cross-linked structure with a slightly rough surface and a porous structure (Fig. 1c and d), which facilitates the rapid transportation of electrolytes and electrons. Therefore, PA-PPy as an interface material is beneficial to improve the electrochemical performance.[29,30] Compared with PA-PPy, the surface morphologies of PA-PPy2 and PA-PPy3 (see Supplementary Fig. S1) were similar to Fig. 1c and d, which proves the successful doping of phytic acid. To prove the doping of phytic acid more visually, EDS scanning analyses were performed on PPy and PA-PPy (Fig. 2). The element distribution diagram of PPy (Fig. 2a) indicated that PPy was primarily composed of C, N and O and without P, while the same EDS scanning results of PA-PPy revealed the presence of P with 7.4% (wt.%) (Fig. 2b). The results proved that the phytic acid molecules were successfully doped into PPy, and this conclusion also consistent with the Fourier transform infrared spectrum in Fig. 3.

The black line in Fig. 3 shows the characteristic peaks of PPy. The absorption peaks at 1550 cm^{-1} and 1400 cm^{-1} were related to the asymmetric and symmetric ring tensile vibration of C-N and C-C, respectively. The absorption peak at 1170 cm^{-1} was caused by the in-plane bending vibration of C-H, while the absorption peak at 1020 cm^{-1} was attributed to the in-plane deformation vibration of C-H and N-H.
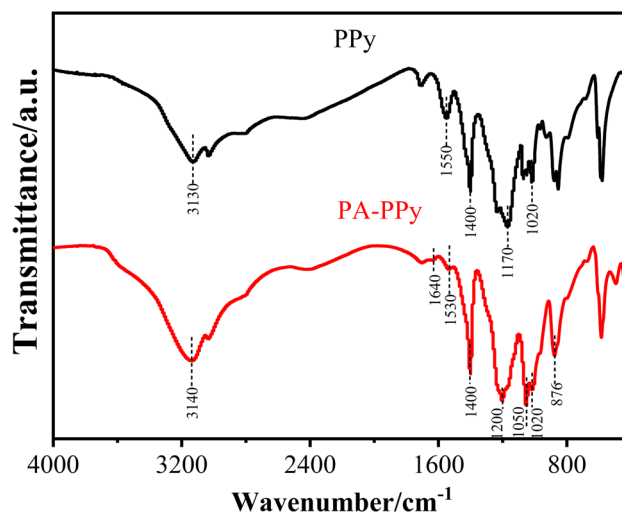

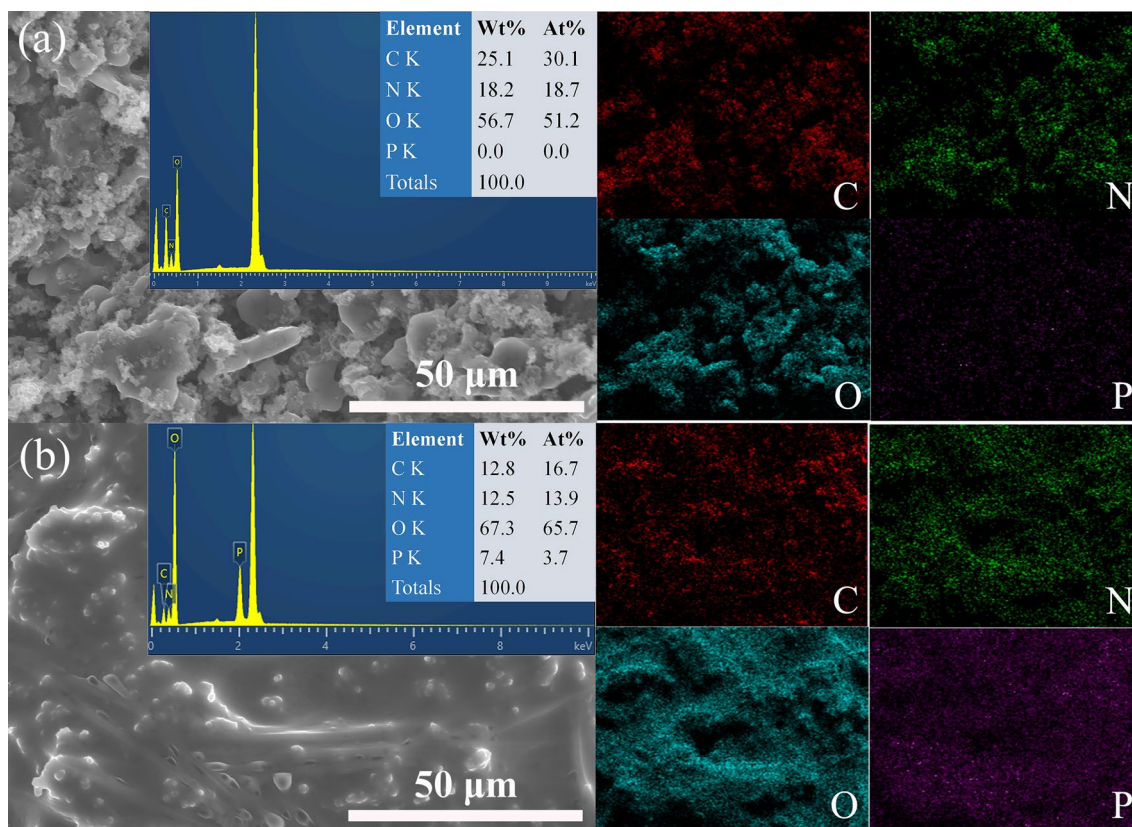**Fig. 3** FTIR spectra of PPy (black line) and PA-PPy composite (red line) (Color figure online).

Fig. 2 EDS mapping of (a) PPy and (b) PA-PPy composites.

In addition, the absorption at 3130 cm⁻¹ was caused by O-H stretching vibration.[31] When phytic acid was doped into PPy, some new absorption peaks appeared in the FTIR spectra (the red line in Fig. 3). The absorption peaks at 876 cm⁻¹, 1050 cm⁻¹, 1200 cm⁻¹ and 1640 cm⁻¹ were attributed to the vibrations of P-O-C, PO_4^{3-}, P=O and HPO_4^{2-} bonds, respectively.[32] Moreover, compared with PPy, the absorption peak at 3140 cm⁻¹ was increased significantly and also accompanied by a peak offset. This phenomenon may be related to the vibration of the O-H bond in phytic acid. All these peaks indicated the presence of phytic acid in the composite material.[30,33]

Hydrophilic Testing of the PA-PPy

As an important medium connecting inorganic electrode with solution, the hydrophilicity of interface material is critical to the electrochemical reaction and the transfer of electrolytes and electrons. By comparing the contact angles of the working electrode on bare SPCE and PA-PPy@SPCE (see Supplementary Fig. S2), we found that the contact angle of PA-PPy@SPCE was about 32°, which was significantly lower than bare SPCE (133.5°). This result suggested that PA-PPy with good wettability can improve the hydrophilicity of the printed carbon paste electrode, which is beneficial for the enrichment of heavy metals and the rapid transfer of electrons during electrochemical testing.

Selection of Electrochemical Detection Technique

DPASV, SWASV, LSASV and SCASV were compared for the detection of Pb^{2+} under the same conditions, and the results are shown in Fig. S3. It can be seen from the figure that the peak responses of SWASV, LSASV and SCASV were lower than the detection of DPASV. Therefore, DPASV was selected as the subsequent detection technique.

DPASV mainly includes an enrichment stage, static stage and dissolution stage. Firstly, a negative constant potential was applied to promote the diffusion of HMIs to the electrode surface and the reduction of these migrated HMIs.[34] Then the system was kept stationary for a period to ensure that the mass transfer on the electrode surface and in the solution reached a steady state and to improve the repeatability of the analysis results. Lastly, forward potential was applied to oxidize the enriched metals into ionic states.[30] Stripping current and stripping potential were recorded to achieve a qualitative and quantitative analysis.

DPASV Performance of Different Sensors

Figure 4a depicts the DPASV curve of PA-PPy@SPCE in the absence of Pb^{2+} (purple line) and the DPASV curves of PPy@SPCE (red line), PA-PPy@SPCE (blue line), and bare SPCE (black line) in the presence of 150 nM Pb^{2+} under the same conditions. It can be seen from the figure that the PA-PPy@SPCE has an obvious electrochemical response signal compared with the PPy@SPCE and bare SPCE. The stripping peak of PA-PPy@SPCE is between −0.7 V and −0.8 V, which is attributed to the dissolution of Pb. The significant enhancement of peak current may be attributed to the phosphoric group in the phytic acid, which can be complexed with Pb^{2+}. The cyclic voltammetry curve clearly shows an obvious redox peak, which corresponds to lead's reduction and dissolution potential (see Supplementary Fig. S4). Furthermore, phytic acid contains a large number of negatively charged functional groups that can improve the adsorption capacity of Pb^{2+}. Hence, the PA-PPy composites can accelerate electron transfer in the detection of Pb^{2+} when phytic acid combines with conductive PPy polymer.[34] The influence of different phytic acid doping concentration on the detection of Pb^{2+} under same condition was compared in Fig. S5. It can be seen that the peak current increased with the doping of phytic acid, but there was virtually no growth when the proportion of $V_A : V_B$ was set to 1:2.

Optimization of Experimental Parameters

In order to achieve the best performance, we optimized the experimental parameters, including buffer pH, deposition potential and deposition time. Figure 4b shows the current response with buffer pH ranging from 3.6 to 6.0. The dissolution peak current increased while the pH was less than 5.6, which might be attributed to the protonation of hydrophilic groups on the sensor.[30] On the contrary, the current decreased when the buffer pH exceeded 5.6. This phenomenon could be caused by Pb^{2+} hydrolysis or the formation of metal hydroxide complexes, both of which affect lead enrichment and dissolution.[35,36] Therefore, we chose 5.6 as the best pH condition for electrochemical tests in subsequent tests. Figure 4c depicts the current responses under various deposition potentials ranging from −1.0 V to −1.6 V, with the current peaking at −1.5 V. This increase might be related to the potential increasing the enrichment ability of Pb^{2+} and thus leading to the increased dissolution. The decrease could be related to hydrogen evolution and other by-products in the solution, which limit the availability of the active site and ultimately affect the dissolution signal.[37] Hence, −1.5 V was selected for the DPASV tests. Lastly, we optimized the deposition time from 60 s to 300 s (Fig. 4d). The peak current increased with the increase of deposition time, while the slope decreased noticeably after 180 s. This might be attributed to the saturation of the binding sites on the electrode surface, which can no longer enrich more Pb^{2+}. So we optimized the deposition time to 180 s during the tests.
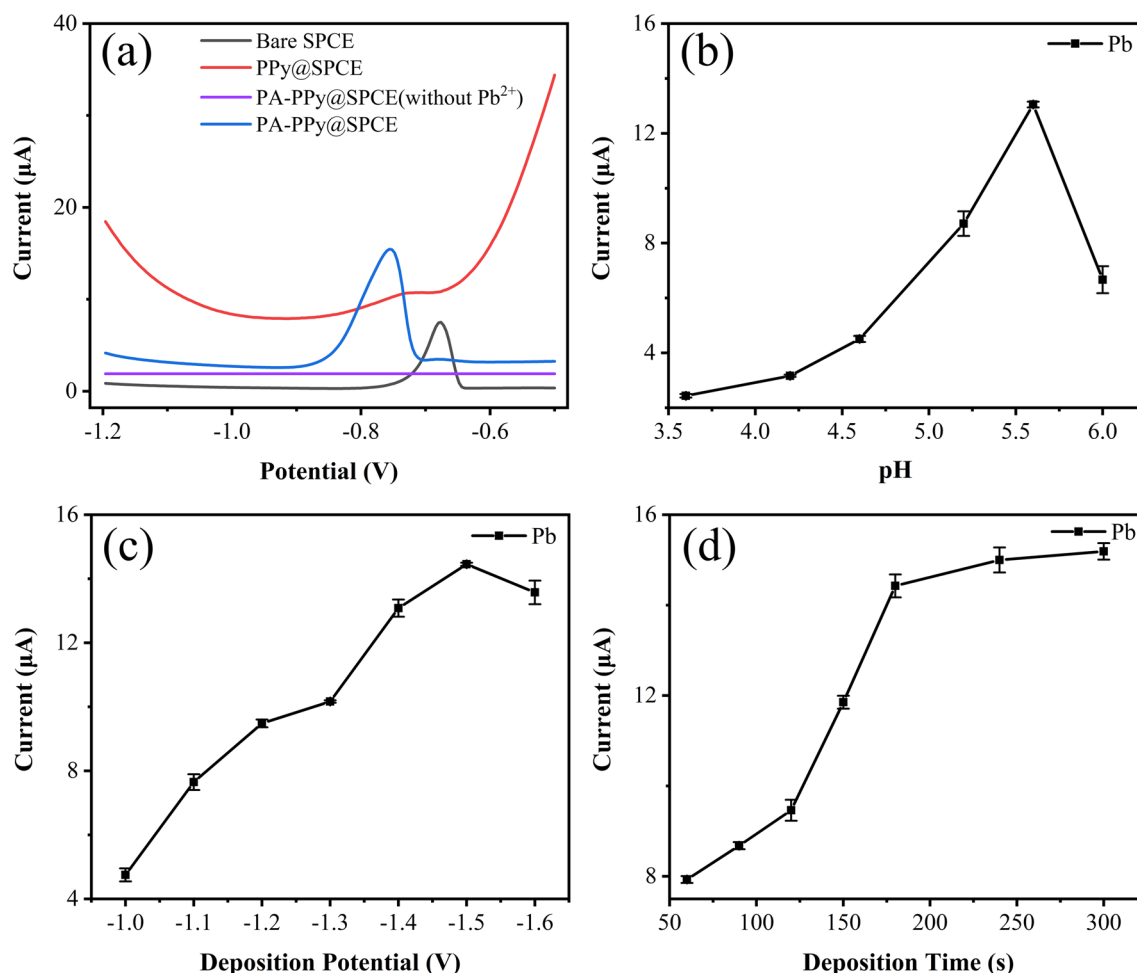
Fig. 4 (a) DPASV curve of PA-PPy@SPCE in the absence of Pb^{2+} (purple line) and the DPASV curves of PPy@SPCE (red line), PA-PPy@SPCE (blue line), and bare SPCE (black line) in the presence of 150 nM Pb^{2+} under the same conditions. The effects of (b) pH, (c) deposition potential and (d) deposition time on Pb^{2+} (150 nM) detection with PA-PPy@SPCE. Error bar: $n = 3$ (Color figure online).

Electrochemical Detection of Pb^{2+}

Under optimal experimental conditions, the DPASV tests of PA-PPy@SPCE were performed at a concentration gradient of 10–600 nM and are shown in Fig. 5a. A clear and sharp oxidation stripping peak was obtained, and the peak current increased along with the Pb^{2+} concentration. According to the DPASV curves, we delineated a good linear relationship between concentration and current (Fig. 5b). The limit of detection (LOD) was calculated to be 0.43 nM, which is lower than the WHO standard of 48.3 nM. Table I shows the comparison of electrochemical Pb^{2+} detection with different sensors. In comparison to previous works, we were able to use a simple, all-solution method to quickly prepare a disposable sensor for the detection of Pb^{2+}, and the sensor has good performance in terms of linear range, detection limit, and stability. Furthermore, our disposable sensor can be used in conjunction with microfluidic technology to detect Pb^{2+} (see Supplementary Figure S6).

Stability, Repeatability and Anti-Interference

The DPASV tests were used to evaluate the stability, repeatability, and immunity to interference of the PA-PPy@SPCE sensor for the detection of Pb^{2+} under optimal experimental conditions, and the results are shown in Fig. 6. The curves essentially maintain coincidence after 20 repetitions (Fig. 6a), with a relative standard deviation (RSD) of about 3.1%, indicating that the sensor is stable. We put the electrode through rigorous testing for a week, and the results showed that the sensor efficiency was essentially above 83% with an RSD of less than 5% (Fig. 6b), indicating that the sensor still performed well during the week of storage, demonstrating the sensor's good stability. The repeatability was carried out with five different PA-PPy@SPCE sensors, and the stripping current values were stable with RSD of about 2% (Fig. 6c). For anti-interference detection, Zn^{2+}, Ni^{2+}, Cr^{6+}, Na^+, K^+, Hg^{2+}, Cu^{2+}, SO_4^{2-}, NO_3^-, NH_4^+ and Cl^- were selected as the interference ions, and the results
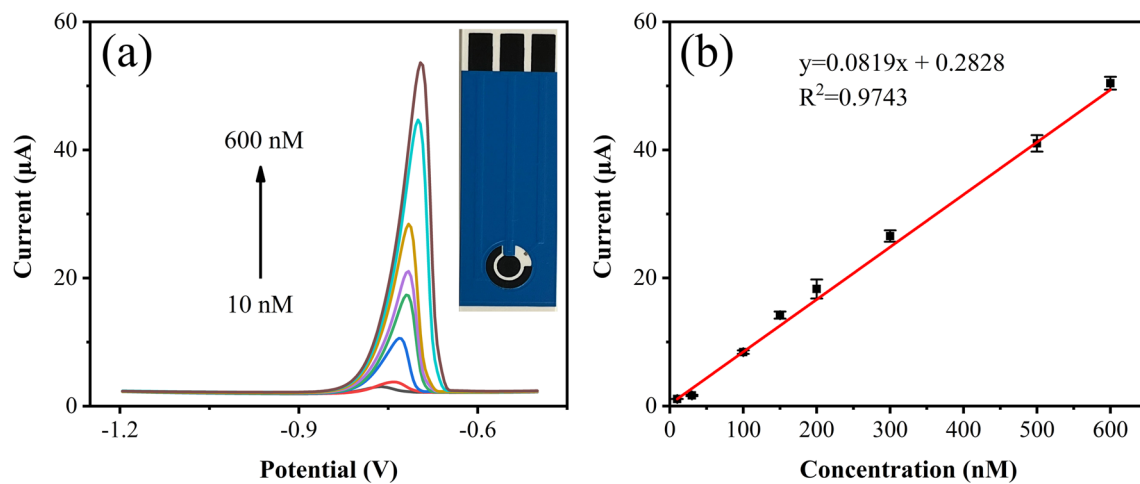
Fig. 5 (a) DPASV curves of PA-PPy@SPCE with different concentrations of Pb^{2+}(Inset is SPCE); (b) linear fitting of concentration and peak current. Error bar: $n=3$.

Table I Electrochemical detection of Pb^{2+} with different modified electrodes

Modified electrode	Technique	Liner range (nM)	Detection limit of Pb^{2+}		References
			Detection limit (nM)	Calculation method	
GDY/GCE	SWASV	$10–10^3$	1.72	3 SD/k	38
EDTA-PPy/SWNTs/SSE	DPV	$150–8\times10^5$	70	3.3 SD/k	39
TGDY/GCE	SWASV	100–1500	5	$S/N=3$	40
OPE/BiONPs/PANI/SPCE	SWV	0–4030	13.5	3 SD/k	41
AuNPs/SPGE	SWASV	96.5–965.3	10.62	$S/N=3$	42
Au@PANI/GCE	SWASV	24–724	3	$S/N=3$	43
Nafion/G/PANI/SPCE	SWASV	4.8–1447.9	0.48	$S/N=3$	44
Bi-SPCNTE	ASV	9.7–482.6	0.97	3 SD/k	45
G/MWCNTs/GCE	DPASV	2.4–144.8	2.41	$S/N=3$	46
PA-PPy/SPCE	DPASV	10–600	0.43	$S/N=3$	This work

S/N is the signal-to-noise ratio; SD is the standard deviation of the multiple blank measurements; k is the slope of the calibration curve.

are shown in Fig. 6d. Normally, the relative change of the target HMI oxidation peak current was within $\pm 10\%$ while the interference ion concentration was 10 times that of the target HMIs, so it can be considered to have little influence on the detection results.[47,48]

For the PA-PPy@SPCE sensor, Hg^{2+} and Cu^{2+} caused more than $\pm 10\%$ change, while the other ions were both within $\pm 10\%$. The presence of Hg^{2+} may form a mercury film on the electrode surface under negative voltage during the test.[49] The small peak near the Pb^{2+} dissolution peak with the presence of Cu^{2+}, which could be the formation of intermetallic alloy, will also affect the detection of Pb^{2+}.[40,50] Hence, some masking agents must be employed to alleviate the interference of Hg^{2+} and Cu^{2+} during the detection of Pb^{2+}.[51–53] As shown in supplementary Fig. S7, the presence of masking agents can reduce Hg^{2+} and Cu^{2+} interference on

Pb^{2+} detection, and the masking agent itself has less interference on Pb^{2+} detection.

Real Sample Analysis

The practical application of the PA-PPy@SPCE sensor was investigated using the markup method with tap water as the sample. The tap water sample and HAc-NaAc solution were mixed in a 1:1 ratio during the test. There was no obvious peak without Pb^{2+} addition. With the addition of different concentrations of standard solutions, a significant increase can be observed. The results of the spiked test are summarized in Table II. Meanwhile, the ICP-MS method was employed to detect Pb^{2+} in real samples for comparison. The results demonstrated that the proposed method was compatible with the traditional method ($R^2=0.996$)
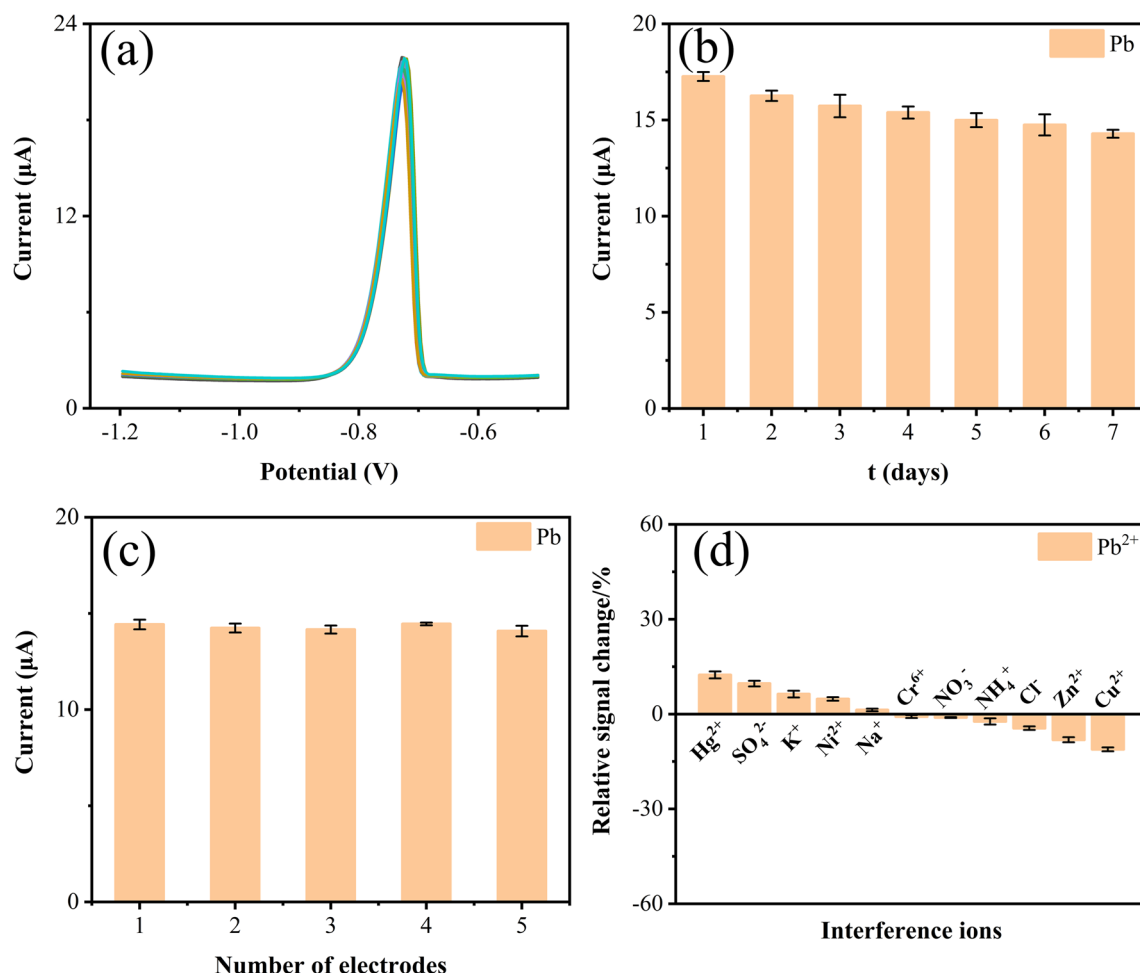
Fig. 6 (a) DPASV response of PA-PPy@SPCE electrode to Pb^{2+} with 20 repetitions; (b) effect of storage time on PA-PPy@SPCE electrode for the detection of Pb.$^{2+}$. (c) DPASV currents of PA-PPy@SPCE for five different electrodes; (d) the interference test of PA-PPy@SPCE in the presence of 10 times the interference ions. Error bar: $n = 3$.

Table II The detection of Pb^{2+} in an actual water sample

Sample	Added (nM)	Found (nM)	Recovery (%)	RSD (%)
Tap water	0	0	–	–
	150	148.4	98.9	2.8
	200	197.3	98.6	1.8
	300	279.5	93.2	2.4

(see Supplementary Fig. S8), proving that the sensor could be applied to the detection of Pb^{2+} in actual water sources.

Conclusions

Combining the full solution method and SPCE, we prepared a disposable electrochemical sensor for lead ion detection with *in situ* polymerization of conductive PA-PPy. During the polymerization of PPy, the negatively charged phytic acid functional molecules can be adsorbed into polypyrrole by electrostatic action. The results show that phytic acid functionalized PPy was beneficial for the detection of Pb^{2+} with its unique characteristics and the PA-PPy@SPCE sensor represented excellent detection performance from 10 nM to 600 nM with good stability (RSD = 3.1%), repeatability (RSD < 2%), and lower detection limit (LOD = 0.43 nM). Moreover, we successfully employed the PA-PPy@SPCE sensor to realize the detection of tap water with a good recovery rate (> 93%). Combined with a simple preparation method, screen printing technology and microfluidic technology, large-scale lead sensors can be fabricated. However, further advancements in the types, range, and convenience of detecting heavy metals are still required. We will continue to optimize the interface materials, improve the sensor preparation process, and develop a portable electrochemical detection device to detect a variety of trace heavy metals simultaneously and *in situ*.

References

1. J. Godt, F. Scheidig, C. Grosse-Siestrup, V. Esche, P. Brandenburg, A. Reich, and D.A. Groneberg, The toxicity of cadmium and resulting hazards for human health. *J. Occup. Med. Toxicol.* 1, 22 (2006).

2. F. Zahir, S.J. Rizwi, S.K. Haq, and R.H. Khan, Low dose mercury toxicity and human health. *Environ. Toxicol. Pharmacol.* 20, 351 (2005).

3. T.W. Clarkson, L. Magos, and G.J. Myers, The toxicology of mercury—current exposures and clinical manifestations. *N. Engl. J. Med.* 349, 1731 (2003).

4. M. Farouz, S.I. El-Dek, M.M. ElFaham, and U. Eldemerdash, Ecofriendly sustainable synthetized nano-composite for removal of heavy metals from aquatic environment. *Appl. Nanosci.* 12, 1585 (2022).

5. Y. Zhao, X. Yang, P. Pan, J. Liu, Z. Yang, J. Wei, W. Xu, Q. Bao, H. Zhang, and Z. Liao, All-printed flexible electrochemical sensor based on polyaniline electronic ink for copper(II), lead(II) and mercury(II) ion determination. *J. Electron. Mater.* 49, 6695 (2020).

6. J. Garcia-Leston, J. Mendez, E. Pasaro, and B. Laffon, Genotoxic effects of lead: an updated review. *Environ. Int.* 36, 623 (2010).

7. J.P. Chen, L. Wang, and S.-W. Zou, Determination of lead biosorption properties by experimental and modeling simulation study. *Chem. Eng. J.* 131, 209 (2007).

8. B. Devadas, M. Sivakumar, S.-M. Chen, M. Rajkumar, and C.-C. Hu, Simultaneous and selective detection of environment hazardous metals in water samples by using flower and christmas tree like cerium hexacyanoferrate modified electrodes. *Electroanalysis* 27, 2629 (2015).

9. A. Munir, A. Shah, J. Nisar, M.N. Ashiq, M.S. Akhter, and A.H. Shah, Selective and simultaneous detection of Zn^{2+}, Cd^{2+}, Pb^{2+}, Cu^{2+}, Hg^{2+} and Sr^{2+} using surfactant modified electrochemical sensors. *Electrochim. Acta* 323, 134592 (2019).

10. S.Y. Guang, G. Wei, Z.Q. Yan, Y.H. Zhang, G. Zhao, R.L. Wu, and H.Y. Xu, A novel turn-on fluorescent probe for the multichannel detection of Zn^{2+} and Bi^{3+} with different action mechanisms. *Analyst* 143, 449 (2018).

11. G.C. Zhu, Y. Li, and C.Y. Zhang, Simultaneous detection of mercury(II) and silver(I) ions with picomolar sensitivity. *Chem. Commun.* 50, 572 (2014).

12. M. Shellaiah, T. Simon, P. Venkatesan, K.W. Sun, F.H. Ko, and S.P. Wu, Nanodiamonds conjugated to gold nanoparticles for colorimetric detection of clenbuterol and chromium(III) in urine. *Microchim. Acta* 185, 1 (2018).

13. Z.Q. Yan, H. Yuan, Q. Zhao, L. Xing, X.Y. Zheng, W.G. Wang, Y.L. Zhao, Y. Yu, L. Hu, and W.L. Yao, Recent developments of nanoenzyme-based colorimetric sensors for heavy metal detection and the interaction mechanism. *Analyst* 145, 3173 (2020).

14. H. Huang, W.C. Zhu, X.C. Gao, X.Y. Liu, and H.Y. Ma, Synthesis of a novel electrode material containing phytic acid-polyaniline nanofibers for simultaneous determination of cadmium and lead ions. *Anal. Chim. Acta* 947, 32 (2016).

15. H.Y. Lv, Z.Y. Teng, S.C. Wang, K. Feng, X.L. Wang, C.Y. Wang, and G.X. Wang, Voltammetric simultaneous ion flux measurements platform for Cu^{2+}, Pb^{2+} and Hg^{2+} near rice root surface: utilizing carbon nitride heterojunction film modified carbon fiber microelectrode. *Sens. Actuators B Chem.* 256, 98 (2018).

16. G. Zhu, Y. Li, and C.-Y. Zhang, Simultaneous detection of mercury(II) and silver(I) ions with picomolar sensitivity. *Chem. Commun.* 50, 572 (2014).

17. Q. Zhang, Q. Du, M. Hua, T. Jiao, F. Gao, and B. Pan, Sorption enhancement of lead ions from water by surface charged polystyrene-supported nano-zirconium oxide composites. *Environ. Sci. Technol.* 47, 6536 (2013).

18. Q. Peng, J. Guo, Q. Zhang, J. Xiang, B. Liu, A. Zhou, R. Liu, and Y. Tian, Unique lead adsorption behavior of activated hydroxyl group in two-dimensional titanium carbide. *J. Am. Chem. Soc.* 136, 4113 (2014).

19. W. Deng, W. Tan, Z. Fang, Q. Xie, Y. Li, X. Liang, and S. Yao, ABTS-multiwalled carbon nanotubes nanocomposite/Bi film electrode for sensitive determination of Cd and Pb by differential pulse stripping voltammetry. *Electroanalysis* 21, 2477 (2009).

20. J.G. Manjunatha, M. Deraman, N.H. Basri, and I.A. Talib, Fabrication of poly(Solid Red A) modified carbon nano tube paste electrode and its application for simultaneous determination of epinephrine, uric acid and ascorbic acid. *Arab. J. Chem.* 11, 149 (2018).

21. C. Raril and J.G. Manjunatha, Fabrication of novel polymer-modified graphene-based electrochemical sensor for the determination of mercury and lead ions in water and biological samples. *J. Anal. Sci. Technol.* 11, 3 (2020).

22. L. Cui, J. Wu, and H. Ju, Electrochemical sensing of heavy metal ions with inorganic, organic and bio-materials. *Biosens. Bioelectron.* 63, 276 (2015).

23. Y. Song, C. Bian, J. Hu, Y. Li, J. Tong, J. Sun, G. Gao, and S. Xia, Porous polypyrrole/graphene oxide functionalized with carboxyl composite for electrochemical sensor of trace cadmium(II). *J. Electrochem. Soc.* 166, B95 (2019).

24. Z.-Y. Guo, X.-S. Yuan, H.-Z. Geng, L.-D. Wang, L.-C. Jing, and Z.-Z. Gu, High conductive PPy-CNT surface-modified PES membrane with anti-fouling property. *Appl. Nanosci.* 8, 1597 (2018).

25. S. Konwer, R. Boruah, and S.K. Dolui, Studies on conducting polypyrrole/graphene oxide composites as supercapacitor electrode. *J. Electron. Mater.* 40, 2248 (2011).

26. V. Sliesarenko, V. Tomina, O. Dudarko, M. Bauman, A. Lobnik, and I. Melnyk, Functionalization of polymeric membranes with phosphonic and thiol groups for water purification from heavy metal ions. *Appl. Nanosci.* 10, 337 (2020).

27. S. Yan, B. Luo, J. He, F. Lan, and Y. Wu, Phytic acid functionalized magnetic bimetallic metal–organic frameworks for phosphopeptide enrichment. *J. Mater. Chem. B* 9, 1811 (2021).

28. C. Hao, R.-H. Yin, Z.-Y. Wan, Q.-J. Xu, and G.-D. Zhou, Electrochemical and photoelectrochemical study of the self-assembled monolayer phytic acid on cupronickel B30. *Corros. Sci.* 50, 3527 (2008).

29. Y. Wang, W.-B. Ma, L. Guo, X.-Z. Song, X.-Y. Tao, L.-T. Guo, H.-L. Fan, Z.-S. Liu, Y.-B. Zhu, and X.-Y. Wei, Phytic acid-doped poly(aniline-co-pyrrole) copolymers for supercapacitor electrodes applications. *J. Mater. Sci. Mater. Electron.* 31, 6263 (2020).

30. N. Wang, H. Dai, D. Wang, H. Ma, and M. Lin, Determination of copper ions using a phytic acid/polypyrrole nanowires modified glassy carbon electrode. *Mater. Sci. Eng. C Mater. Biol. Appl.* 76, 139 (2017).

31. N. Su, H.B. Li, S.J. Yuan, S.P. Yi, and E.Q. Yin, Synthesis and characterization of polypyrrole doped with anionic spherical polyelectrolyte brushes. *Expr. Polym. Lett.* 6, 697 (2012).

32. F. Pan, X. Yang, and D. Zhang, Chemical nature of phytic acid conversion coating on AZ61 magnesium alloy. *Appl. Surf. Sci.* 255, 8363 (2009).

33. H. Dai, N. Wang, D. Wang, H. Ma, and M. Lin, An electrochemical sensor based on phytic acid functionalized polypyrrole/graphene oxide nanocomposites for simultaneous determination of Cd(II) and Pb(II). *Chem. Eng. J.* 299, 150 (2016).

34. H. Hou, K.M. Zeinu, S. Gao, B. Liu, J. Yang, and J. Hu, Recent advances and perspective on design and synthesis of electrode materials for electrochemical sensing of heavy metals. *Energy Environ. Mater.* 1, 113 (2018).

35. S. Anandhakumar, J. Mathiyarasu, and K.L.N. Phani, In situ bismuth film modified carbon fiber microelectrode for nanomolar detection of cadmium and lead. *Indian J. Chem. Sect. A Inorg. Bio-Inorg. Phys. Theor. Anal. Chem.* 51, 699 (2012).

36. Y. Pu, Y. Wu, Z. Yu, L. Lu, and X. Wang, Simultaneous determination of Cd^{2+} and Pb^{2+} by an electrochemical sensor based on $Fe_3O_4/Bi_2O_3/C_3N_4$ nanocomposites. *Talanta Open* 3, 100024 (2021).

37. C. Guo, C. Wang, H. Sun, D. Dai, and H. Gao, A simple electrochemical sensor based on $rGO/MoS_2/CS$ modified GCE for highly sensitive detection of Pb(II) in tobacco leaves. *RSC Adv.* 11, 29590 (2021).

38. Y. Li, H. Huang, R. Cui, D. Wang, Z. Yin, D. Wang, L. Zheng, J. Zhang, Y. Zhao, H. Yuan, J. Dong, X. Guo, and B. Sun, Electrochemical sensor based on graphdiyne is effectively used to determine Cd^{2+} and Pb^{2+} in water. *Sens. Actuators B Chem.* 332, 129519 (2021).

39. M.A. Deshmukh, G.A. Bodkhe, S. Shirsat, A. Ramanavicius, and M.D. Shirsat, Nanocomposite platform based on EDTA modified Ppy/SWNTs for the sensing of Pb(II) Ions by electrochemical method. *Front. Chem.* 6, 1 (2018).

40. X. Guo, Y. Li, H. Huang, D. Wang, R. Cui, J. Li, Y. Zhao, D. Wang, H. Yuan, J. Dong, and B. Sun, Triazine-graphdiyne with well-defined two kinds of active sites for simultaneous detection of Pb^{2+} and Cd^{2+}. *J. Environ. Chem. Eng.* 10, 107159 (2022).

41. E.C. Okpara, S.C. Nde, O.E. Fayemi, and E.E. Ebenso, Electrochemical characterization and detection of lead in water using SPCE modified with BiONPs/PANI. *Nanomaterials* 11, 1294 (2021).

42. H. Wan, Q. Sun, H. Li, F. Sun, N. Hu, and P. Wang, Screen-printed gold electrode with gold nanoparticles modification for simultaneous electrochemical determination of lead and copper. *Sens. Actuators B Chem.* 209, 336 (2015).

43. Z. Lu, W. Dai, B. Liu, G. Mo, J. Zhang, J. Ye, and J. Ye, One pot synthesis of dandelion-like polyaniline coated gold nanoparticles composites for electrochemical sensing applications. *J. Colloid Interface Sci.* 525, 86 (2018).

44. N. Ruecha, N. Rodthongkum, D.M. Cate, J. Volckens, O. Chailapakul, and C.S. Henry, Sensitive electrochemical sensor using a graphene-polyaniline nanocomposite for simultaneous detection of Zn(II), Cd(II), and Pb(II). *Anal. Chim. Acta* 874, 40 (2015).

45. U. Injang, P. Noyrod, W. Siangproh, W. Dungchai, S. Motomizu, and O. Chailapakul, Determination of trace heavy metals in herbs by sequential injection analysis-anodic stripping voltammetry using screen-printed carbon nanotubes electrodes. *Anal. Chim. Acta* 668, 54 (2010).

46. H. Huang, T. Chen, X. Liu, and H. Ma, Ultrasensitive and simultaneous detection of heavy metal ions based on three-dimensional graphene-carbon nanotubes hybrid electrode materials. *Anal. Chim. Acta* 852, 45 (2014).

47. J. Liao, J. Zhang, C.-Z. Wang, and S. Lin, Electrochemical and density functional theory investigation on the differential behaviors of core-ring structured $NiCo_2O_4$ nanoplatelets toward heavy metal ions. *Anal. Chim. Acta* 1022, 37 (2018).

48. Y. Li, R. Cui, H. Huang, J. Dong, B. Liu, D. Zhao, J. Wang, D. Wang, H. Yuan, X. Guo, and B. Sun, High performance determination of Pb^{2+} in water by 2,4-dithiobiuret-reduced graphene oxide composite with wide linear range and low detection limit. *Anal. Chim. Acta* 1125, 76 (2020).

49. X.-Y. Xiao, S.-H. Chen, S.-S. Li, J. Wang, W.-Y. Zhou, and X.-J. Huang, Synergistic catalysis of N vacancies and similar to 5 nm Au nanoparticles promoted the highly sensitive electrochemical determination of lead(II) using an Au/N-deficient-C_3N_4 nanocomposite. *Environ. Sci. Nano* 6, 1895 (2019).

50. Z. Zhai, N. Huang, H. Zhuang, L. Liu, B. Yang, C. Wang, Z. Gai, F. Guo, Z. Li, and X. Jiang, A diamond/graphite nanoplatelets electrode for anodic stripping voltammetric trace determination of Zn(II), Cd(II), Pb(II) and Cu(II). *Appl. Surf. Sci.* 457, 1192 (2018).

51. L. Xiao, S. Zhou, G. Hu, H. Xu, Y. Wang, and Q. Yuan, One-step synthesis of isoreticular metal–organic framework-8 derived hierarchical porous carbon and its application in differential pulse anodic stripping voltammetric determination of Pb(II). *RSC Adv.* 5, 77159 (2015).

52. M. Jarczewska, E. Kierzkowska, R. Ziolkowski, L. Gorski, and E. Malinowska, Electrochemical oligonucleotide-based biosensor for the determination of lead ion. *Bioelectrochemistry* 101, 35 (2015).

53. D. Yang, L. Wang, Z. Chen, M. Megharaj, and R. Naidu, Investigation of copper(II) interference on the anodic stripping voltammetry of lead(II) and cadmium(II) at bismuth film electrode. *Electroanalysis* 25, 2637 (2013).

Authors and Affiliations

Hengchao Zhang[1] · **Yarou Li**[1] · **Yupan Zhang**[1] · **Junfeng Wu**[1,2] · **Shixin Li**[1] · **Lanlan Li**[1,2]

1   College of Mechanical and Electrical Engineering, Henan Agricultural University, Zhengzhou 450002, China

2   Henan International Joint Laboratory of Laser Technology in Agriculture Sciences, Zhengzhou 450002, China